Optical Materials 58 (2016) 171–182

Contents lists available at ScienceDirect

Optical Materials

journal homepage: www.elsevier.com/locate/optmat

Synthesis, Z-Scan and Degenerate Four Wave Mixing characterization of certain novel thiocoumarin derivatives for third order nonlinear optical applications

K. Jayakrishnan [a, *], Antony Joseph [b], K. Paulson Mathew [c], T.B. Siji [c], K. Chandrasekharan [d], N.K. Siji Narendran [d], M.A. Jaseela [e], K. Muraleedharan [e]

[a] Department of Physics, MES College Ponnani, Ponnani South, Kerala, 679 586, India
[b] Department of Physics, University of Calicut, Calicut University, Kerala, 673 635, India
[c] Laboratory for Sustainable Science, Department of Chemistry, St. Thomas College Trissure, Kerala, 680 001, India
[d] Lasers and Nonlinear Optics Laboratory, Department of Physics, National Institute of Technology, Calicut, 673 601, India
[e] Department of Chemistry, University of Calicut, Calicut University, Kerala, 673 635, India

ARTICLE INFO

Article history:
Received 19 April 2016
Received in revised form
22 May 2016
Accepted 23 May 2016

Keywords:
Coumarin
Nonlinear absorption
Third order susceptibility
Optical limiting
Structure optimization

ABSTRACT

The third order nonlinear optical features of certain novel thiocoumarin derivatives have been studied. Single beam Z-scan study on these compounds reveals that the compounds exhibit self defocusing effect upon irradiation with 532 nm, 7 ns pulses of Nd:YAG laser. Nonlinear absorption coefficient, nonlinear refractive index and second-order molecular hyperpolarizability values were estimated. The optical power limiting properties of the compounds are found to be attributable to both two-photon and excited state absorption. Some of the samples show nonlinear absorption coefficient (β_{eff}) as high as 24.5 cm/GW. UV–Visible and photoluminescence outputs of these compounds reveal remarkable absorptive and emissive properties. This article also reports extraordinary growth of third order optical nonlinearity in pure coumarin upon certain donor substitutions in lieu of hydrogen. Degenerate Four Wave Mixing (DFWM) signals of the compounds were analyzed to verify the Z-scan results. Electrostatic Surface Potential (ESP) mapping and structure optimization techniques have been employed to interpret the structure-property relationship of each molecule.

1. Introduction

Nonlinear optical processes in conjugated organic molecular systems have led to compelling technological promises in terms of novel high performance materials and devices [1–3]. At the microscopic scale, the π-electron excitations occurring in the individual molecular units are the essential dynamics that control the observed optical nonlinearity in majority of the organic compounds. Vivid strategies have been reported by various research groups to enhance the nonlinear optical features of conjugated organic molecular systems [4]. Each scheme has its own merits and demerits. But, ever since the development of such strategies in the early 1960's [5,6] till date, none has met out with an all pervading solution to the entire specification issues stipulated by the nonlinear optical (NLO) device fabricators [7]. However, many molecular systems have managed to attain satisfactory levels of thermal, mechanical and chemical stability by offering superlative degree of optical figure of merit in terms of transparency and nonlinear optical coefficients at many wavelengths [8,9].

Among the various classes of compounds investigated, coumarin based molecular systems are a scarcely studied compound for its nonlinear applications, whereas many of its derivatives are widely investigated for various other photo physical applications [10–12]. Many of the coumarin derivatives are extensively used for commercial production of fluorescent dyes, deodorants, skin lotions, and as gain medium in dye laser cavities [13,14]. They show a broad variety of pharmacological activities like anti-inflammatory, antibiotic, antidiabetic, and antidepressant activities [15]. Such compounds are also known for their photochemical and photophysical properties. Especially, pure coumarin can undergo a reversible photo induced cyclodimerisation upon irradiation at wavelength $\lambda > 300$ nm, leading to cyclobutane based

* Corresponding author.
E-mail address: jayakrishnan.mes@gmail.com (K. Jayakrishnan).

http://dx.doi.org/10.1016/j.optmat.2016.05.039
0925-3467/

dimers with four possible isomeric configurations [16]. Resultantly, such molecular systems with pendant groups can give rise to polymeric formations upon irradiation with $\lambda > 300$ nm. Such polymeric systems embedded with coumarin fragments are being used in photoactive surface applications, electroluminescence, photo-alignment of liquid crystalline molecules and reversible two-photon optical data storage [17]. Computational methods using semiempirical techniques have demonstrated that coumarin and its sulphur derivatives (thiocoumarin) possess well-defined dipole moments [18]. In addition, the thiocoumarin versions crystallize in non-centrosymmetric space groups and this feature is responsible for its enhanced second harmonic generation (SHG) properties [19]. Pure coumarin with phenylpropenoyl and dimethylamino substitution at the 3-position have been previously studied by our own group in PMMA matrix and their NLO responses have been reported [20].

We hereby report the generation of third order optical nonlinearity like nonlinear absorption and four-wave mixing in certain thiocoumarin derivatives in its solution form. Interestingly, the contrast study among pure coumarin (CM-1) and the newly prepared thiocoumarin versions revealed feeble nonlinear optical response from the former. This article illustrates how the substitution of different electron donors/acceptor moieties at the 3-positions and sulphur at the 2-position (thiocoumarin) does facilitate the enhancement of nonlinear response in coumarin based molecular systems. In this paper, we discuss the preparation of different thiocoumarin derivatives and the measurements of the nonlinear optical absorption and refraction effects in these compounds by Z-scan and Degenerate Four Wave Mixing (DFWM) techniques. The optical limiting efficiency of the compounds has also been presented.

2. Experimental

2.1. Materials and methods

All the chemicals used were of analytical grade. Dimethyl Formamide (DMF), coumarin (2*H*-chromen-2-one), salicylaldehyde and Na_2SO_4 were procured from Sigma-Aldrich. β-oxodithioester was prepared by the modification of an already reported procedure [21]. Solvents like ethyl acetate and n-hexane were synthetically pure and further purified by double distillation. Fourier Transform Infra-Red spectra of the compounds were recorded with Jasco 410 (Resolution 0.9642 cm^{-1}) using KBr disc. Linear absorption spectra were taken with SCHIMADZU 2450 PC in spectroscopic grade DMF. Perkin Elmer Fluorescence spectrophotometer (LS-55) was used to record the photoluminescence (PL) spectra of the samples. Abbe refractometer tuned for 532 nm wavelength was used to measure linear refractive index (n_0). Nd:YAG laser (Quanta-Ray INDI), delivering 7 ns pulses at a repetition rate of 10 Hz was used to measure both real and imaginary part of the third order nonlinear optical susceptibility constants. Rj-7620 energy ratio meter (Laser Probe Inc, USA) was used to compare input and output pulses of temporally Gaussian profiled beam.

2.2. Synthesis of compounds

2.2.1. CM-1(2H-chromen-2-one)

Pure coumarin used as procured from Sigma-Aldrich. Anal.Calc for $C_9H_6O_2$: C, 73.97; H, 4.14; O, 21.9; UV–vis: λ_{max}/nm (DMF)~275. FT-IR:ν_{max}/cm^{-1} (KBr phase) 753(ring vib.), 781 (C–C stretching vib), 912 (O–C vib.), 1186 (-C-C vib.), 1371 (C–H stretching), 1598 (–C–C– stretching), 2360 (C═O stretching), 3047 (═C–H stretching vib.), 3427 (-OH stretching).

2.2.2. CM-2 (2H chromene-2-thione)

The β-oxodithioester (1.0 mmol), salicylaldehyde (1.2 mmol) and triethylamine (10 mol %) were mixed and heated at 80 °C for 1 h. After completion of the reaction (monitored by TLC), ethyl acetate (10 mL) was added to the reaction mixture, and the catalyst was filtered off. Water (20 mL) was then added to the reaction mixture and the mixture extracted with ethyl acetate (20 mL). The combined organic layers is dried over anhydrous Na_2SO_4 and then evaporated in vacuum. The crude residue is purified by column chromatography over silica gel using ethyl acetate:hexane (5:1) as eluent to afford the 2*H*-chromene-2-thiones. Yield: 82%.Anal.Calc for C_9H_6OS: C, 66.64; H, 3.73; O, 9.86; S, 19.77; UV–vis: λ_{max}/nm (DMF) ~272, 376. FT-IR:ν_{max}/cm^{-1} (KBr phase) (See Figs. 1 and 2) 592(ring deform. Vib.), 749 (–C–H out of plane def. vib.), 1095 (–C═C stretching), 1205 (C–H deformation), 1252 (-C-O stretching), 1551 (in plane ring vib.), 1724 (–C═O str. vib.), 3051 (═C–H str. vib) [21].

2.2.3. CM-3 (3-benzoyl-2H-chromene-2-thione)

β-oxodithioester derived from acetophenone on reaction with salicylaldehyde gives 3-benzoyl-2*H*-chromene-2-thione as a yellow solid. Yield: 90%.Anal.Calc for $C_{16}H_{10}O_2S$:C, 72.45; H, 6.08; O, 10.72; S, 10.75; UV–vis: λ_{max}/nm (DMF)~269, 313, 385. FT-IR:ν_{max}/cm^{-1} (KBr phase) 593 (ring deformation vib.), 646 (C–S stretch. vib.), 761 (–C–H deform. vib.), 959 (–C–H out of plane vib.), 1450 (comb. of C═O and C═C str. Vib.), 1557 (in plane ring vib.), 1604 (C–C str. vib.), 1664 (–C═O stretching vib.), 3063 (═C–H str. vib.), 3423 (-OH stretch. vib.).

2.2.4. CM-4 (3-(4-bromobenzoyl)-2H-chromene-2-thione)

β-oxodithioester derived from *p*-bromoacetophenone on reaction with salicylaldehyde gives 3-(4-bromobenzoyl)-2*H*-chromene-2-thione as a yellow solid. Yield: 87%. Anal. Calc for $C_{16}H_9BrO_2S$: C, 55.67; H, 2.63; Br, 23.15; O, 9.27; S, 9.29; UV–vis: λ_{max}/nm (DMF) ~ 279, 386. FT-IR:ν_{max}/cm^{-1} (KBr phase) 572 (C–Br stretching), 763(aromatic C–H out of plane def. vib.), 1019(C–H def. vib.), 1175(–C═O stretching vib.),1243(–C–H def. vib.), 1351 (C═S stretching vib.), 1598 (-C-C stretching vib.), 2813 (C–H stretching), 2357 (–C═C stretching), 2925 (C–H stretching symmetric.), 3428 (–OH stretching).

2.2.5. CM-5 (3-naphthoyl-2H-chromene-2-thione)

The β-oxodithioester derived from 2-acetyl naphthalene on reaction with salicylaldehyde gives 3-naphthoyl-2*H*-chromene-2-thione as a yellow solid. Yield: 88%. Anal.Calc for $C_{20}H_{12}O_2S$: C, 75.93; H, 3.82; O, 10.11; S, 10.14; UV–vis: λ_{max}/nm (DMF) ~ 314, 385. FT-IR:ν_{max}/cm^{-1} (KBr phase) 574 (ring deformation vib.), 695 (–C═S vib.), 753 (out of plane deformation vib.), 911 (–C–H out of plane deformation vib.), 1142 (–C═O stretching), 1227 (C–H deformation vib.), 1371 (C–O stretching), 1552 (C═C stretching in plane vib.), 1598 (–C═C– stretching vib.), 1671 (–C═C stretching), 2923 (–OH stretching), 3030 (═C–H stretching vib.), 3426 (-OH stretching).

3. Results and discussion

3.1. Linear absorption studies

The entire samples exhibit a large transparency beyond 530 nm and the onset of absorption band occurs above 250 nm. Major absorption regions of all the compounds fall in the 250–390 nm range (near-UV), which can be assigned to the absorption of the conjugate chromophores. Fig. 3 shows that all samples are bathochromically shifted with respect to CM-1 whose absorption peak lies at 275 nm. This indicates higher electron delocalization in samples CM-2 to CM-5. Very feeble linear absorption is observed for the samples at

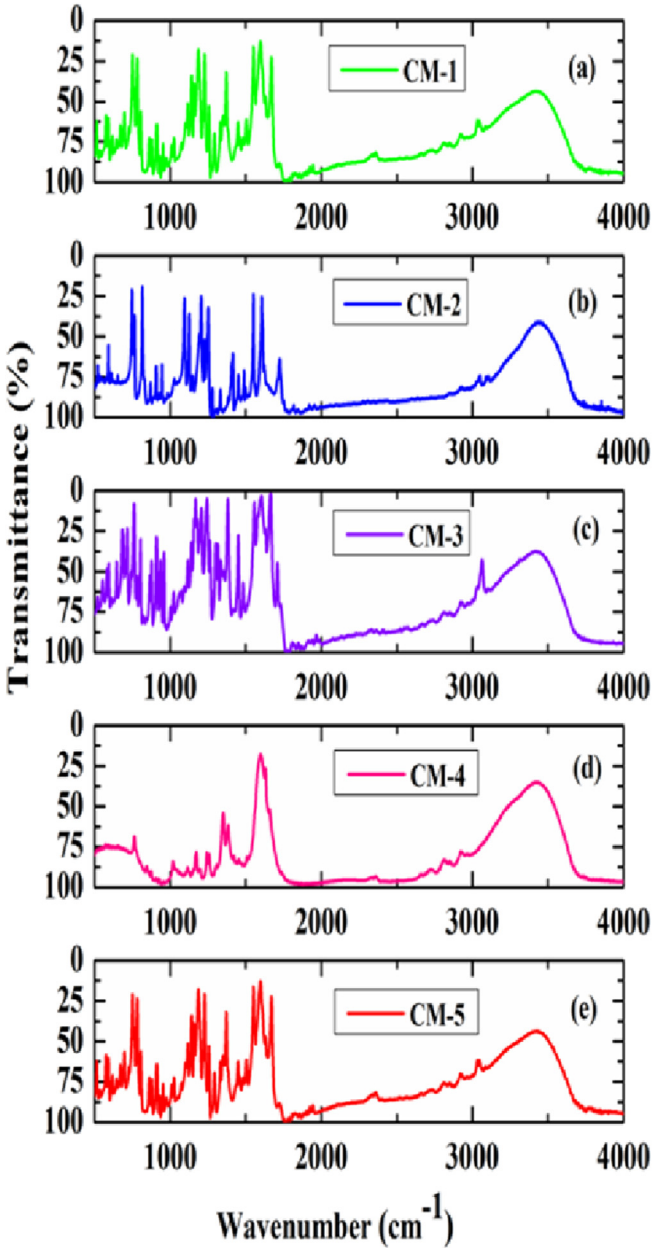

Fig. 1. FTIR spectra of (a) CM-1, (b) CM-2, (c) CM-3, (d) CM-4, (e) CM-5 taken with KBr disc method.

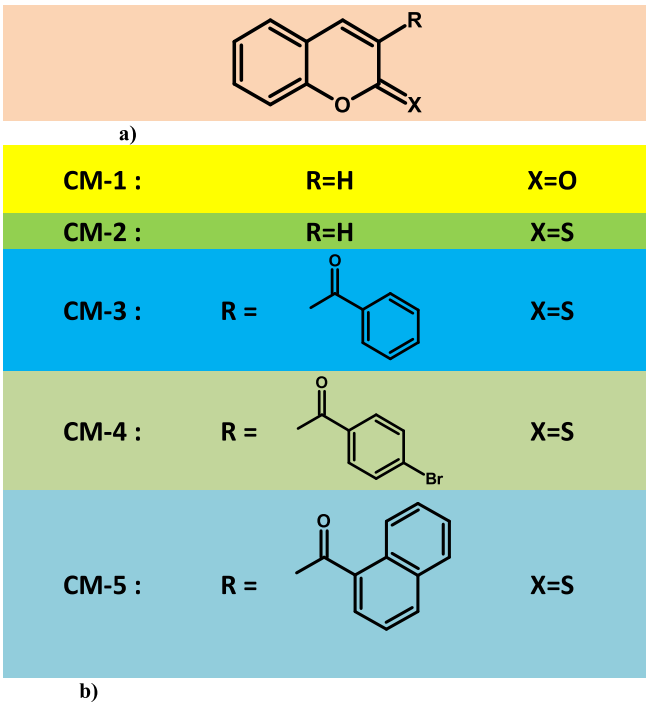

Fig. 2. a) General structure of basic coumarine molecular unit. **b)** Molecular structures of the compounds CM-1 to CM-5.

the excitation wavelength (532 nm). This would give rise to comparatively nonresonant nonlinearity with minimal linear loss. Among the compounds, relative linear absorption at 532 nm is the highest for CM-2 (~0.053). This fact is also obvious from the value of linear absorption coefficient shown in Table 1. Optical band gap of the compounds dissolved in DMF were evaluated from the Tauc plots and are as follows: CM-1 (3.65 eV), CM-2 (2.86 eV), CM-3 (2.82 eV), CM-4 (2.8 eV), and CM-5 (2.81 eV).

Absorption maxima of samples at 272, 275 and 279 can be assigned to the transitions between nonbonding atomic orbitals holding unshared pair of electrons and the antibonding pi-orbitals ($n \rightarrow \pi^*$). These are known as R-band transitions, which are due to the presence of compounds containing double bonds involving hetero-atoms like C═O, C═S etc. These groups often bear unshared pair of electrons. The seemingly enhanced bathochromic shift of CM-4 (386 nm) can be accounted with the increased conjugation of the molecule due to the presence of bromine at the para-position of the phenyl ring. In CM-4, bromine atom is more of a donor-like compared to the oxygen in the >C═O bond. In Section 4, we will see the impeding effect of certain structural features on the conjugation of CM-4.

3.2. Photoluminescent (PL) studies

PL spectra of all samples were recorded in DMF. Since the samples are in liquid phase, phosphorescence could not give rise to the origin of certain spectral emissions; hence the observed signals are purely of fluorescence origin. Many of the coumarin derivatives are efficiently used as fluorescent dyes and considerable attention has been obtained due to their emission in the blue-green region [22,23]. Fluorescent yield of such dyes are highly affected with the polarity and viscosity of the medium. Emission spectra of the coumarin derivatives from their electronically excited states are shown in Fig. 4. From the excited singlet states, the electron is paired by opposite spin to the second electron in the ground-state. Consequently, return to the ground state is spin allowed and occurs rapidly by the emission of photons [24].

Among the studied samples, CM-4 is observed to be a pure monochrome emitter in the visible region with λ_{max} at 555.5 nm. Spectra of other samples fitted to Lorentzian-Gaussian (L-G) [25] and yielded the following wavelength compositions. CM-1: $\lambda_1 = 415.5$ nm (21.9%), $\lambda_2 = 504.9$ nm (6.28%) and $\lambda_3 = 480$ nm (71.8%); CM-2: $\lambda_1 = 500.64$ nm (21.7%), $\lambda_2 = 540.99$ nm (30.08%) and $\lambda_3 = 558.17$ nm (48.3%); CM-3:$\lambda_1 = 475.58$ nm (34.14%), $\lambda_2 = 526.5$ nm (36.82%) and $\lambda_3 = 565.44$ nm (29.06%); CM-4: $\lambda_1 = 555.5$ nm (100.00%); CM-5: $\lambda_1 = 534.82$ nm (63.35%), $\lambda_2 = 493.74$ nm (36.65%). Potential efficiency of the compounds as blue-green emitters is worth notable from the above data.

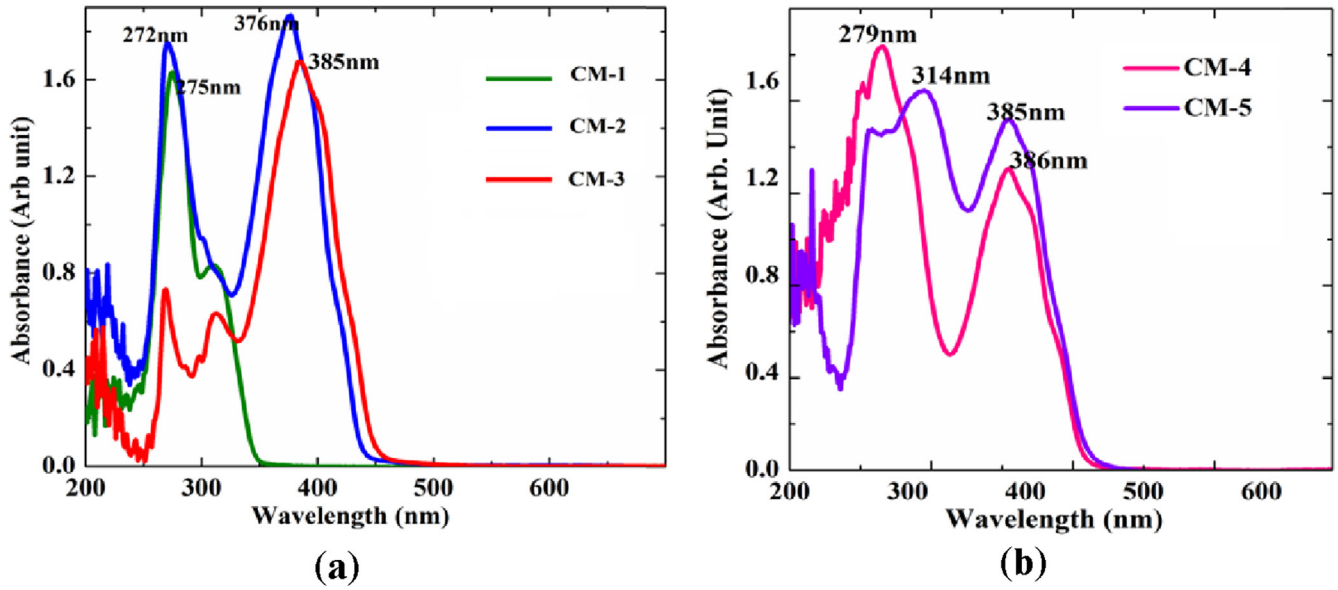

Fig. 3. Linear absorption spectra of coumarin derivatives recorded in DMF solution. a) CM1, CM2 and CM3 b) CM4 and CM-5.

Table 1
Experimentally determined values of T, I_s, n_0, n_2, α_0 and nonlinear absorption coefficient (β_{eff}) for different compounds.

SN	Sample	Linear transmittance (T %)	I_s (GW/cm^2)	n_0	n_2 (10^{-10} esu)	α_0 (cm^{-1})	β_{eff} (cm/GW)
1	CM-1	95.25	0.102	1.401	–	0.49	0.5
2	CM-2	76.12	0.049	1.414	−0.351	2.73	24.5
3	CM-3	81.76	0.075	1.398	−0.349	2.01	12.5
4	CM-4	78.64	0.074	1.413	−0.387	2.40	15.0
5	CM-5	88.01	0.150	1.412	−0.376	1.28	5.0

3.3. Nonlinear optical studies

3.3.1. Open aperture Z-scan studies

Estimation of third-order nonlinear susceptibility coefficients of the compounds involves two stages—measurements of real and imaginary parts. Closed and open aperture Z-scan of the sample yields respectively the real and imaginary part of the third order nonlinear optical susceptibility coefficients $\chi^{(3)}$. Open aperture Z-scan is based on the recording of variation of transmitted optical intensity $T_{open}(z)$ through the sample by the translation of the position (z) of the interaction medium across the focal plane of a tightly focussed Gaussian beam by fixing a pyroelectric detector at the receiving end where all the transmitted light is detected. The detector output provides the information about the nonlinear absorption coefficient (β_{eff}) of the sample. Open aperture Z-scan experiments were performed under optical excitation with 532 nm (2.33 eV), 7 ns pulses as explained in Refs. [26,27]. Fig. 5 shows that the normalized transmittance $T_{open}(z)$ decreases as the sample approaches the focal plane which is indicative of the intensity dependent nonlinear absorption property of the sample. Different samples show varied levels of intensity dependent absorption, with the highest fall in T_{open} (z) recorded by CM-2.

All investigated samples are found to obey the intensity dependant absorption equation of the form [28].

$$\alpha(I) = \frac{\alpha_0}{1+\frac{I}{I_s}} + \beta_{eff} I \tag{1}$$

where α (I), α_0, β_{eff}, and I_s are respectively, the apparent intensity dependent absorption, linear attenuation coefficient, effective two photon absorption coefficient, and saturation intensity (intensity at which linear attenuation drops to half its initial value). For estimating transmitted intensity for a given input irradiance, the beam propagation equation [29],

$$\frac{dI}{dz} = \left[\left(\alpha_0 \Big/ \left(1+\frac{I}{I_s}\right)\right) + \beta_{eff} I\right] I \tag{2}$$

can be numerically solved. From the best fit obtained, I_s and β_{eff} can be extracted and the resulting values for each sample are given in Table 1. Corresponding normalized transmittance $T_{open}(z)$ of the sample (as plotted in Fig. 5) for a temporally and spatially Gaussian beam can be related to the sample position z through the expression [30].

$$T_{open}(z) = \left[\frac{1}{\pi^{1/2} q(z)}\right] \int_{-\infty}^{+\infty} \ln\left[1 + q(z) e^{-\tau^2}\right] d\tau \tag{3}$$

where q(z) is given by the relation $q(z) = [\beta_{eff} I_0 (1 - e^{-\alpha_0 l})]/[1 + (z/z_R)^2]\alpha_0$, with I_0 the maximum incident intensity at z = 0, l = sample thickness and z_R is the Rayleigh distance of the laser beam, defined by $z_R = \pi w_{o^2}/\lambda$, with w_0 representing the beam waist and λ the laser wavelength.

UV–Vis plot shown in Fig. 3 indicates that the intensity dependent nonlinear absorption is likely to arise from both two-photon absorption (2 PA) and excited state absorption (ESA). Z-scan plot of CM-2 shows highest nonlinear absorption coefficient (24.5 cmGW^{-1}) and that of CM-1 shows the least absorption (0.5 cmGW^{-1}). The rest of the samples show values intermediate

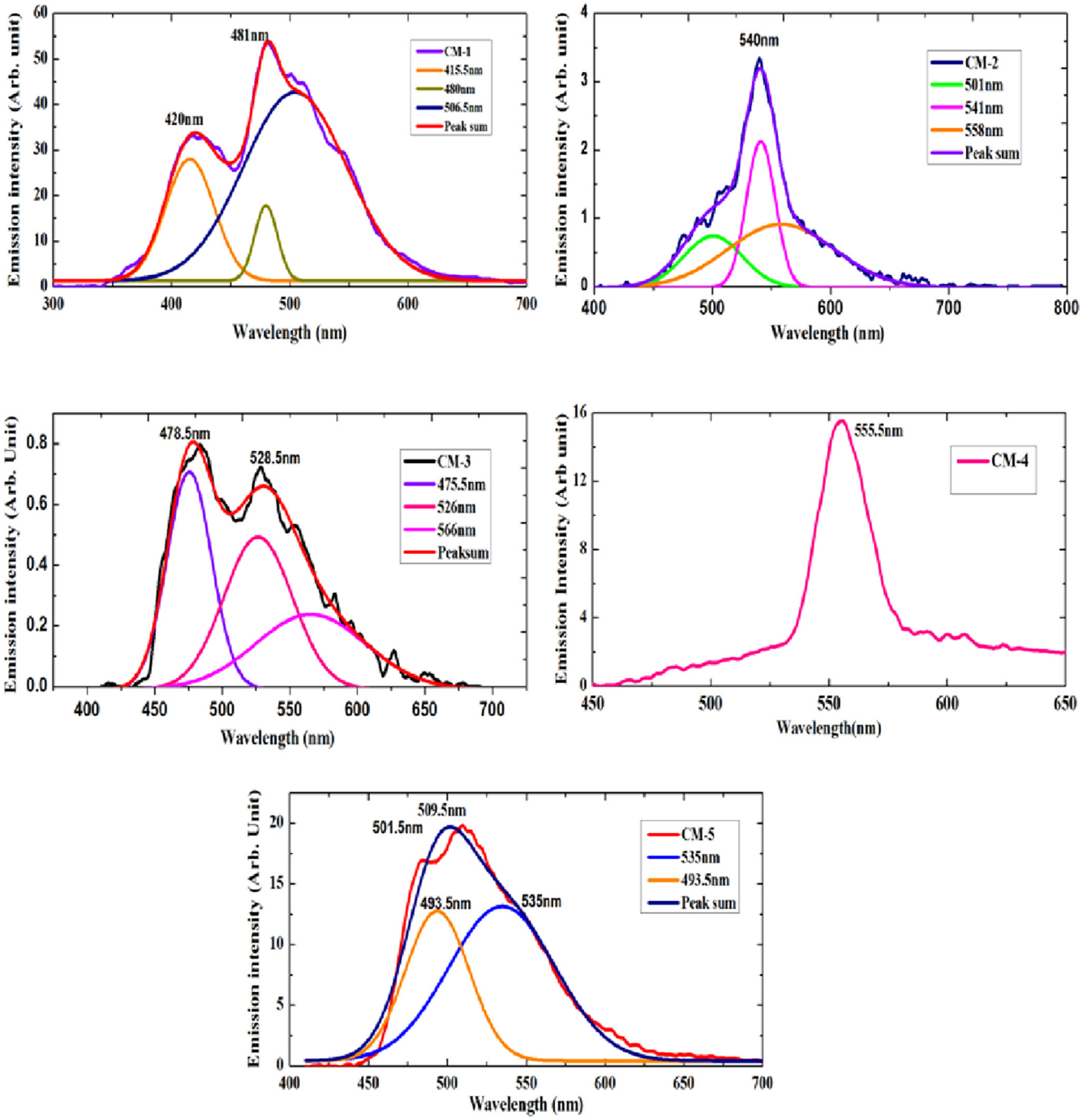

Fig. 4. Deconvoluted PL spectra of coumarin derivatives CM-1 to CM-5.

between that of CM-1 and CM-2. The extraction of β_{eff} enables us to estimate the imaginary part of the third order susceptibility from the relation [31] $\mathrm{Im}\chi^{(3)}(esu) = 10^{-7}c^2n_0^2\beta/96\pi^2\omega$. A weak absorption tail at 532 nm for all the samples render a finite linear absorption coefficient for all the compounds (except CM-1), which are tabulated in Table 1.

3.3.2. Closed aperture Z-scan studies

The closed aperture normalized transmittance T_{closed} (z) traces plotted against the sample position are shown in Fig. 6. We used a pin-hole of radius 2 mm as the aperture. The peak-valley configuration of the Z-scan spectra is indicative of a negative refractive nonlinearity of the compounds CM-2 to CM-5 which could be due to the self de-focusing effect of the Gaussian beam within the sample [27]. Due to the negative nonlinearity of the sample, the overall refractive index of the sample tends to be less than its normal value exhibited in low intensity regime. Gaussian profile of the beam generates a gradient in refractive index with the highest change in effective refractive index Δn at the vicinity of the beam axis and the lowest change at the beam periphery. Hence the distorted wavefront assumes a convex profile which leads to self defocusing of beam within the sample solutions.

The normalized closed aperture transmittance data has been fitted to the relation of the form [32]:

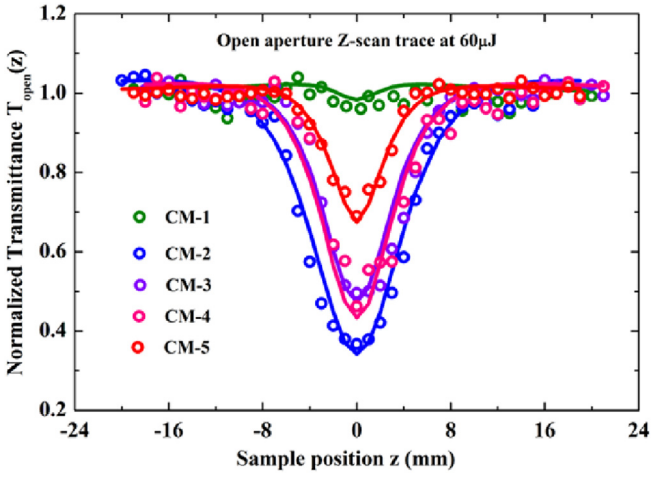

Fig. 5. Open aperture Z-scan traces of samples observed at a concentration of 0.4 (% m/v) in DMF with a fixed on-axis beam intensity $I_0 = 1.66$ GW/cm^2. The solid lines are theoretically fitted with the equation (3). (a) $\beta_{eff} = 0.5$ cmGW^{-1} for CM-1, (b) $\beta_{eff} = 24.5$ cmGW^{-1} for CM-2, (c) $\beta_{eff} = 12.5$ cmGW^{-1} for CM-3, (d) $\beta_{eff} = 15$ cmGW^{-1} for CM-4, (e) $\beta_{eff} = 5$ cmGW^{-1} for CM-5. The circles are experimental data.

$$T(z) = 1 + \frac{4x}{[(x^2+9)(x^2+1)]}\Delta\varphi_0 - \frac{2(x^2+3)}{[(x^2+9)(x^2+1)]}\Delta\psi_0 \tag{4}$$

where $x = z/z_R$ and, the on-axis nonlinear phase shift $\Delta\varphi_0$ is related to the third-order nonlinear refractive index γ through beam intensity I_0 by the relation $|\Delta\varphi_0| = k\gamma L_{eff} I_0$, where, the wave number, $k = 2\pi/\lambda$ and L_{eff} is the effective sample thickness which takes in to account the linear absorption of the sample. Similarly, the on-axis phase shift $\Delta\Psi_0$ given in eqn. (4) is due to nonlinear absorption which is given by the relation $\Delta\psi_0 = \frac{1}{2}\beta I_0 L_{eff}$. The experimental measurements of γ allow us to determine the real part of the third-order nonlinear optical susceptibility $\chi^{(3)}$ from the relation [31] $\mathrm{Re}\chi^{(3)}(esu) = 10^{-6} c n_0^2 \gamma / 480\pi^2$, where c is the speed of light in cms^{-1} and ω is the fundamental frequency of laser beam.

The fitted data shown in Fig. 6 indicates that maximum nonlinear phase shift is for CM-2. Estimated value of nonlinear refractive index n_2 (esu) at the concentration 0.4 (% m/V) for all the samples are shown in Table 1. The value of n_2 in SI system may be obtained by multiplying with 1.4×10^{-14} m^2/W. The closed aperture Z-scan of CM-1 gives no peak-valley configuration; instead it simply gives randomly scattered data points which make it unsuitable for any curve-fitting. But, interestingly, it gives weak DFWM signals and is displayed in Fig. 7 a and b.

3.3.3. Degenerate Four Wave Mixing (DFWM) studies

Variations of the DFWM signal as a function of the input probe intensity for CM-1 to CM-5 are shown in Fig. 7 a) and b). The cubic intensity dependence of the amplitude of the DFWM signal for all the samples is found to follow a similar pattern except in CM-1. The cubic dependence of the signal is found to obey the relation [33].

$$I^{\omega}_{conjugate} \alpha \left(\frac{\omega}{2\varepsilon_0 c^2 n_0^2}\right)^2 \cdot \left|\chi^{(3)}\right|^2 l^2 I^3_{Probe}(\omega) \tag{5}$$

where $I^{\omega}_{conjugate}$ is the phase conjugate DFWM signal intensity, $I_{Probe}(\omega)$ is the probe intensity, and l is the sample thickness. The solid lines in Fig. 7 are the cubic fit to the experimental data. The value of $\chi^{(3)}_{sample}$ can be estimated using Equation (6) for the absorbing media.

The fitting constant value C_{sample} of each compound was extracted from the plots shown in Fig. 7 using the relation $y = C_{sample}.x^3$ [34].

$$\chi^{(3)}_{sample} = \chi^{(3)}_{ref}\left[\frac{C_{sample}}{C_{ref}}\right]^{1/2}\left[\frac{n_{sample}}{n_{ref}}\right]^2 \frac{l_{ref}}{l_{sample}}\left[\frac{\alpha_0 l e^{\frac{\alpha_0 l}{2}}}{(1-e^{-\alpha_0 l})}\right] \tag{6}$$

where the subscript 'ref' refers to the standard reference CS_2 under identical conditions. The $\chi^{(3)}$ value of reference CS_2 is taken to be 1.7×10^{-12} esu at 532 nm [35].

3.3.4. Optical limiting (OL) studies

In an open aperture Z-scan configuration, with the Gaussian beam as the excitation source, if the sample is displaced along the beam axis, then the sample will be exposed to a varying degree of laser fluence at each z value, and fluence will be maximum at the focal plane of the beam. The input laser intensity expressed in GW/cm^2 can be estimated using the relation $I_{input} = 4\sqrt{\log 2}E_{pulse}/\pi^{1/2}\omega^2(z)$ where E_{pulse} is the energy per laser pulse and ω (z) is the beam radius at any arbitrary z position. In order to investigate the optical limiting responses of the samples, normalized transmittance is plotted against the incident laser intensity. Such plots enable us to compare the optical limiting performance of different samples. Optical limiting threshold (OLT) is an important benchmark to compare the performance of samples. OLT signifies the incident beam intensity at which the transmittance falls to half of the linear transmittance (T_H) [36,37]. For an ideal passive optical limiter material, it exhibits constant linear transmittance below threshold and above threshold the transmittance should be momentously cut down and the device must turn down completely opaque. But, with realistic temporal and spatial profiled beams, the output fluence cannot be clamped at a predetermined value and adding to this complexity, there exist some degree of indeterminacy in the activation threshold value of the limiter materials [38].

Using open aperture Z-scan data, optical limiting traces of the samples were plotted and are shown in Fig. 8. Linear transmissions of the solutions were in the range of ~75%–95%. Compounds CM-2, CM-3, CM-4 display reasonable OLT with T_H values respectively in the order of 5.4×10^{12}, 1.09×10^{13}, and 0.8×10^{13} expressed in the unit of W/m^2. The enhanced conjugation of CM-5 with respect to CM-2 is not evident in the optical limiting performance of CM-5. This could be due to the quenching effect of naphthalene moiety attached to the thiocoumarin structure. Many reports point out that naphthalene can act as triplet-triplet transition quencher in many molecules [39,40]. It can be suggested that the excited singlet state of naphthalene lies at a higher energy level than the excited singlet of thiocoumarin but the triplet of naphthalene lies at a lower energy level than that of thiocoumarin. This could lead to a feeble ESA which is ascribable to the weaker OL of CM-5 with reference to CM-2. From Fig. 8, it is also obvious that CM-1 hardly shows any obvious optical limiting property.

Optical limiting has various origins; the phenomena like multiphoton absorption (MPA), excited state absorption (ESA), free carrier absorption (FCA), self-focusing, self-defocusing, two-photon absorption (TPA) etc, can be effectively utilized in designing many passive optical limiting devices. Interplay of two or more of the above cited mechanisms may also lead to OL. Based on the UV–Vis trace and open aperture fit, it can be stated that the OL property of CM-2 is rooted in both TPA and ESA (this includes excited singlet or triplet transition) with major contribution from TPA.

The microscopic third order nonlinear optical parameter of the molecules, known as second order hyperpolarizability (γ_h) was estimated using the relation $\gamma_h = \chi^{(3)}/L^4N$ where N is the density of molecules in the unit of molecules per cm^3 [41] and is presented in

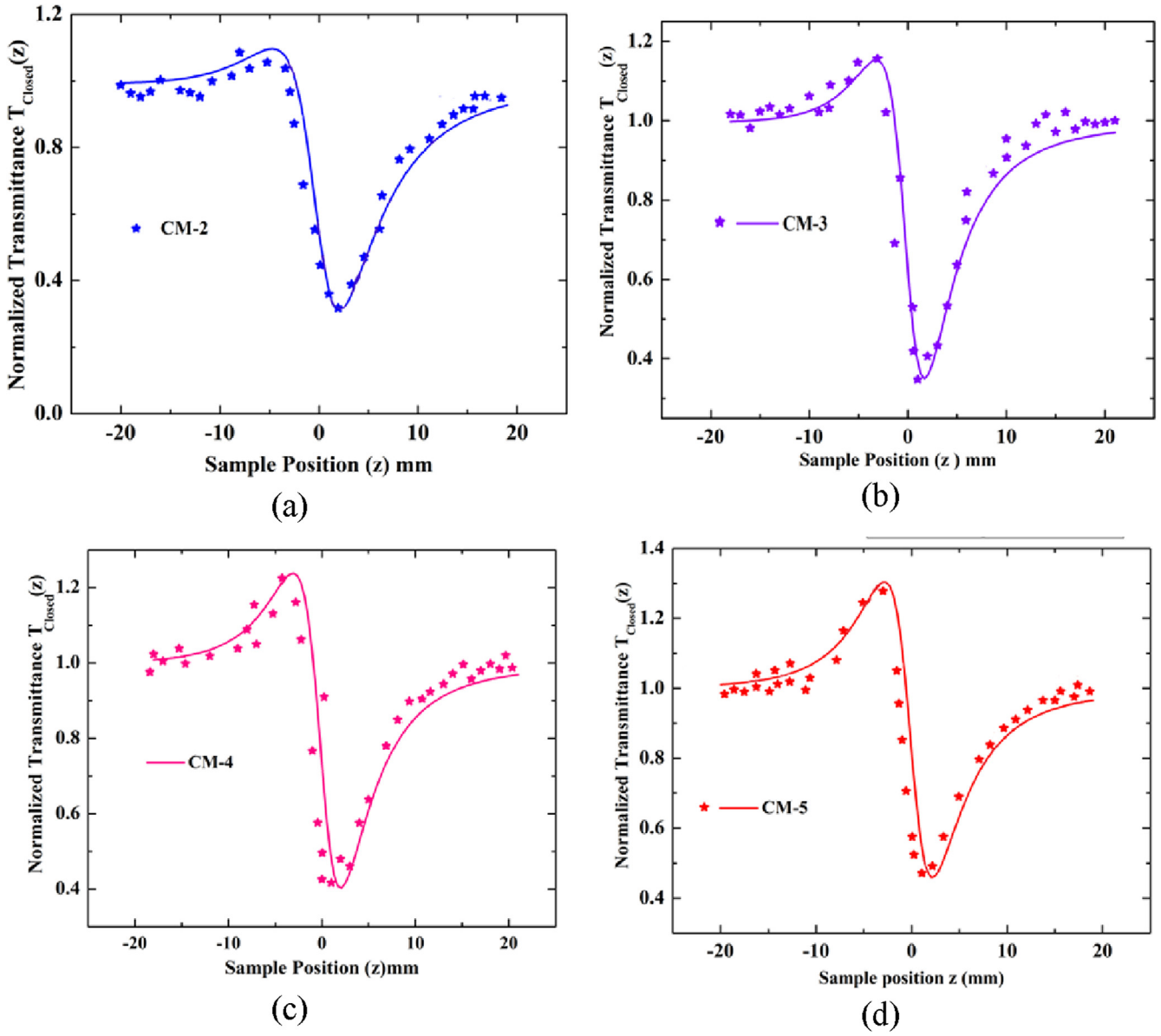

Fig. 6. Closed aperture Z-scans of CM-2 to CM-5 in DMF solution indicating a negative type of nonlinearity at a beam intensity of $I_0 = 1.66$ GW/cm^2. Solid line is a fit of experimental data with $\Delta\Phi_0 = 0.68$ for CM-2, $\Delta\Phi_0 = 0.57$ for CM-3, $\Delta\Phi_0 = 0.41$ for CM-4 and $\Delta\Phi_0 = 0.27$ for CM-5.

Table 2. The term L is the local field factor, which can be expressed in terms of linear refractive index n_0 as: $L = (n_0^2 + 2)/3$. The value of γ_h is recorded to be the highest for CM-4 and lowest for CM-5.

The presence of highly electronegative bromine at the phenyl wing contributes to maximum charge-transfer asymmetry to the molecule CM-4 hence its γ_h value is the highest. The optical figure of merit (F or FOM) is calculated by taking α_0 in to account. FOM is estimated from the relation $\chi^{(3)}/\alpha_0$ [42]. FOM is a measure of the nonlinear response that can be achieved for a given absorption loss and is useful in comparing the performance of different materials in different regions of absorption. Among the samples investigated CM-2 is found to have the highest FOM. The measured $\chi^{(3)}$ value of CM-2 is one order of magnitude greater than that obtained by Sharafudeen et al. in dimethylamino and phenylpropenoyl derivatives of coumarin [20]. Our values are also comparable with the cyclic conjugated structures of porphyrin derivatives and phthalocyanines, which are among the most widely accepted third order organic nonlinear materials. The reported values of third order susceptibility $\chi^{(3)}$ for metal phthalocyanines (Pc), for example, SnPc is of the order of 10^{-12} esu [43] and zinc porphyrin also exhibited similar values [44].

3.3.5. *Reverse saturable absorption mechanism*

The dependence of the effective two-photon absorption coefficient β_{eff} as a function of the incident beam intensity I_0 for all thiocoumarin (TC) compounds for a fixed concentration is shown in Fig. 9. All the traces show that increasing beam intensity results in a decrease of β_{eff}. The fall-off of β_{eff} with increasing I_0 is a consequence of the sequential two-photon absorption which involves ESA also [45]. With the increasing intensity, the total absorption of all the TC solution approaches the absorbance of triplet state. Therefore, the β_{eff} would be found reduced at least up to intensities where no other intensity-dependent processes are involved which can cause the reduction of transmittance in the solution [31,45]. Sample CM-3 and CM-5 show comparatively gentle fall in β_{eff} with increasing I_0. This is because, in addition to ESA, there exists

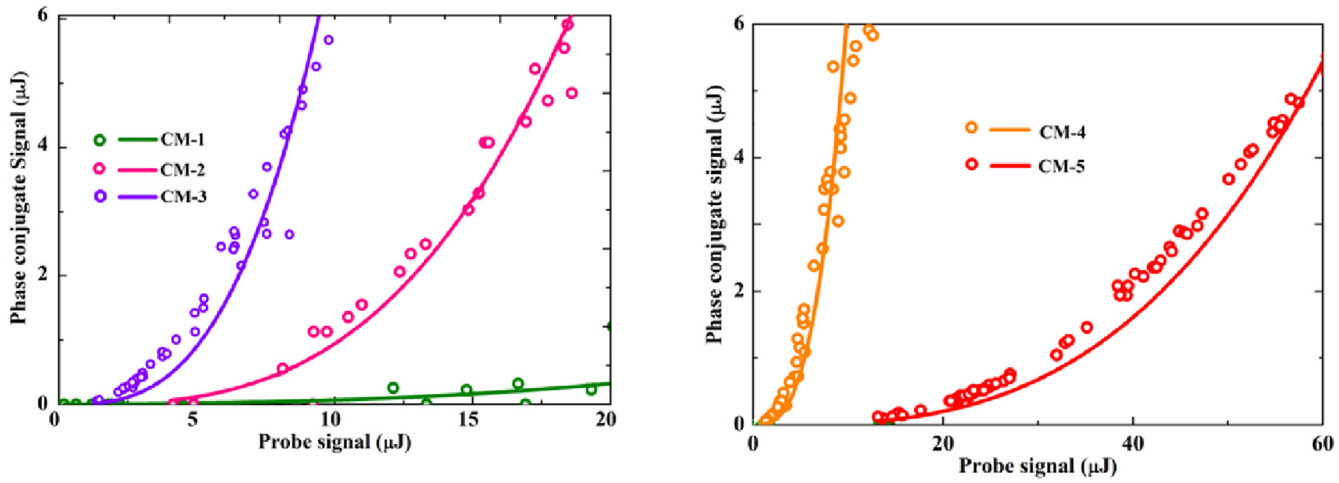

Fig. 7. Probe signal vs. Phase conjugate signal curves for CM-1 to CM-5 in DMF for concentration 0.4 (% m/v). CM-1 shows (marked in green bubbles) feeble DFWM signal which is roughly cubic fittable and CM-4 (shown in orange bubbles) gives highest DFWM signal intensity. (For interpretation of the references to colour in this figure legend, the reader is referred to the web version of this article.)

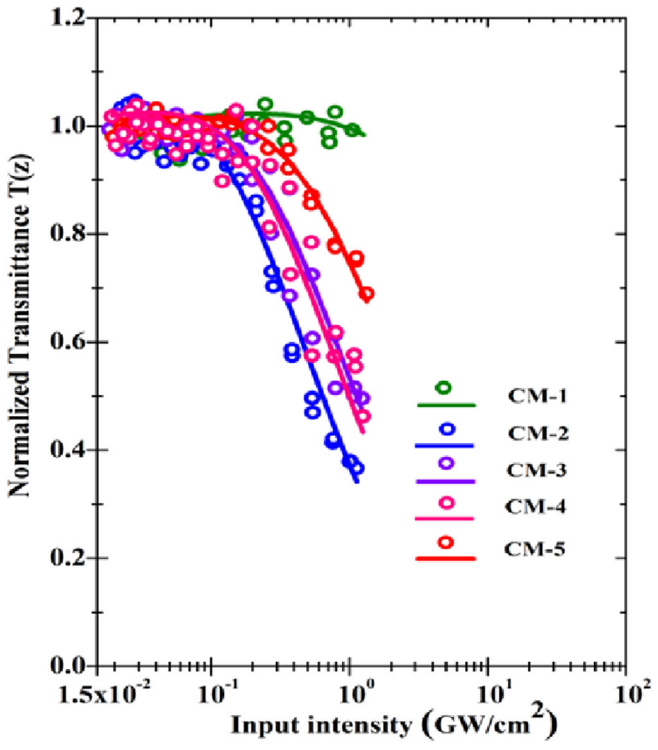

Fig. 8. Optical limiting curves for samples CM-1 to CM-5 at 0.4 (% m/v) concentrations in DMF.

contribution from the pure TPA to the effective nonlinear absorption of both the compounds.

When molecules are photo-excited with 7ns pulses at 532nm, it get excited from the ground state (S_0) into the first excited singlet state (S_1) as illustrated with Jablonski five-level transition diagram shown in Fig. 9 b). As the inter-system crossing rate is high for nanosecond pulses, the molecule in S_1 gets transferred predominantly to the lower level of the triplet state (T_1). T_1 state has a longer lifetime and higher absorption cross-section than that of S_0. After resonantly absorbing single photons, the molecules in T_1 go to higher excited-state T_2. Due to the very short life-time of T_2 (~ps), the molecules can relax back to the lower excited triplet state through collisional energy transfer to the surrounding solvent molecules. This process occurs within the time scale of ns. This non-radiative relaxation results in temperature rise (ΔT) in the sample and leads to the instantaneous refraction change causing an additional refractive index change given by the relation $\Delta n_{thermal} = (\partial n/\partial T)\Delta T$. The resultant non-uniform spatial distribution of refractive index around the beam axis produces a (thermal) lensing effect [46] with either a positive or negative sign, depending on the sign of the thermo-optic coefficient ($\partial n/\partial T$) of the material under study.

3.3.6. Structure-NLO property relationship

We used Gaussian 09 W simulation package [47] for molecular structure analysis. The geometry optimizations of the molecules were performed with 6–31 g (d, p) as basis set and computational procedures were carried out via DFT (B3LYP) method [48,49].

Table 2
Experimentally determined values of $Re\chi^{(3)}$, $Im\chi^{(3)}$, effective third order susceptibility coefficients $\chi^{(3)}$ and γ_h determined with Z-scan and DFWM techniques.

Compound	Z-Scan					DFWM
	Re $\chi^{(3)}$ (x10^{-12} esu)	Im $\chi^{(3)}$ (x10^{-12} esu)	$\chi^{(3)}$ (x10^{-12} esu)	F (x10^{-12} esu cm)	γ_h (x10^{-31} esu)	$\chi^{(3)}$ (x10^{-12} esu)
CM-1	–	0.11	0.11	0.25	0.02	0.43
CM-2	5.19	5.26	7.39	2.71	1.58	6.15
CM-3	5.18	2.62	5.81	2.88	2.13	5.00
CM-4	5.80	3.22	6.63	2.76	3.02	4.98
CM-5	5.64	1.09	5.75	4.50	2.41	2.92

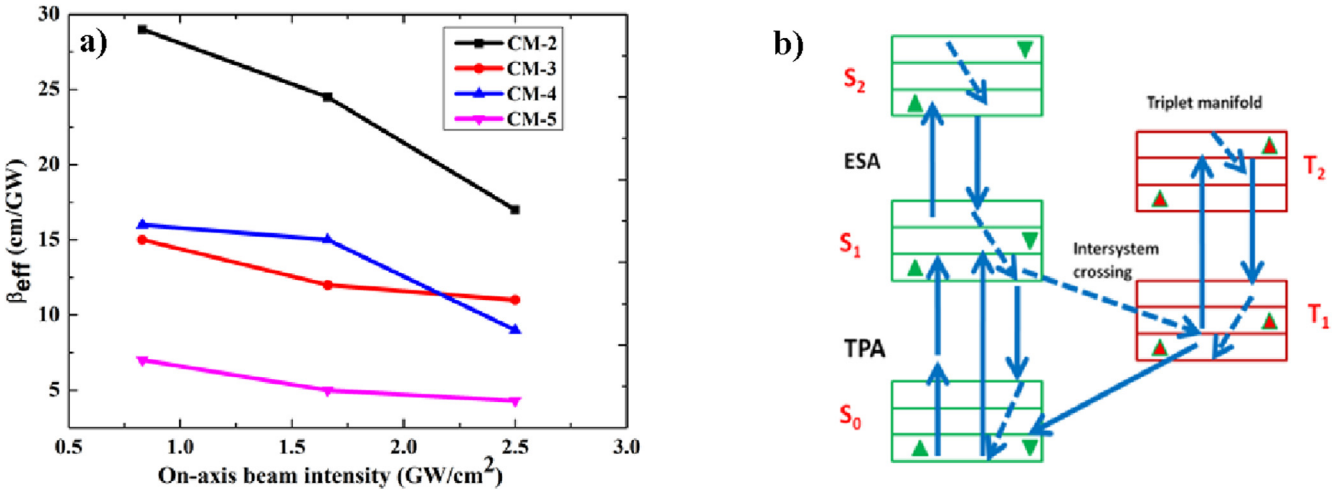

Fig. 9. a) β_{eff} versus on-axis beam intensity I_0 for CM-2, CM-3, CM-4 and CM-5 in DMF solution for three different energies. Concentrations of all sample solutions were kept identical. **b)** Jablonski diagram showing both TPA and RSA. ESA indicates the excited state absorption. The dotted arrows indicate non-radiative internal conversion. Singlet (S) state electrons are in opposite spin orientation and Triplet (T) state electrons have identical spins.

Computational thermo chemical studies based on isodesmic reactions of some aromatic compounds suggest that CM-1 can be considered to be a pure aromatic system because of the presence of delocalized benzene ring [50]. The computed outputs show that (see Table 3) highest occupied molecular orbital (HOMO) energy of CM-1 and CM-2 are −6.5 eV and −5.9 eV respectively. It implies that substitution of sulphur in place of oxygen has direct impact on reducing HOMO-LUMO energy gap. This accounts for why CM-2 is having more delocalized π-electron cloud than CM-1. Fig. 10 f), g) and j) display the optimized structures of CM-3, CM-4 and CM-5 molecules. It suggests that these molecules are non-planar. Possible explanation of such a non-planarity is the steric effect between thiocoumarin ring and the substituted ring. From the optimization plot (Fig. 10 d), it is obvious that thiocoumarin ring is almost planar, however the substitution with C═O group moiety in the remaining molecules is slightly out of plane with respect to the thiocoumarin base-structure as inferred from the computed values of dihedral angle, which varied from 10° to 25° for the remaining molecules (see Table 3). Among the five molecules analyzed, we found that CM-5 holds the highest dihedral angle with a value of 22.5°, while, CM-3 and CM-4 yield values 10.6° and 9.8° respectively.

Furthermore, the bridged C═O bond is having an estimated bond length of 1.22 A° which can only be attributed to 'pure' C═O double bond and not to a 'delocalized' C═O double bond which requires a mandatory bond length of the order of ~1.55 A°. These values indicate that the conjugation is not likely to be extended from thiocoumarin moiety to substituted ring(s) through bridged C═O group. Hence, it can be concluded that the presence of non-planar alternating double bonds containing C═O group as substituents to thiocoumarin ring cannot contribute to the extension of π-electron conjugation as expected in a typical π-conjugated system. In the ESP plots shown in Fig. 10, higher electron density is marked with thicker blue shade. ESP plots of CM-1 and CM-2 shown in Fig. 10 a) and c) indicate that spatial spread of electron cloud is more in CM-2 than in CM-1; with the obvious reason that sulphur, in CM-2 is size-wise larger and less electronegative than its oxygen counterpart in CM-1. This enlarged electron cloud spread provides with an enhanced dipolar interaction to CM-2 with the incident laser field. In rest of the molecules, the π-electron extension is compensated with the increasing dihedral angle as shown in Table 3. Comparatively low value of nonlinear optical parameters, like $\chi^{(3)}$ and β_{eff} of these molecules (with respect to CM-2) can be ascribed to this effect (see Tables 1 and 2).

Table 3
Theoretically calculated values of E_{HOMO}, E_{LUMO}, and Dihedral angle with B3LYP/6-31G (d, p) in gas phase.

Molecule	Dihedral angle (in degrees)	E_{HOMO} (eV)	E_{LUMO} (eV)
CM1	–	−6.5	−1.9
CM2	–	−5.9	−2.3
CM3	10.6	−6.0	−2.5
CM4	9.8	−6.1	−2.6
CM5	22.5	−5.8	−2.5

E_{HOMO}: Highest Occupied Molecular Orbital, E_{LUMO}: Energy of Lowest Unoccupied MO.

4. Conclusion

Our report reveals how the newly derived thiocoumarin derivatives act as promising third order nonlinear materials with varying degree of optical limiting property. Third order nonlinear optical coefficients have been extracted through single beam Z-scan technique using 7 ns, 10 Hz, 532 nm Nd:YAG laser. An attempt has been made to explore and explain the relationship that exists between their molecular structures and the third order NLO response using ESP plots and structure optimization techniques. The third order NLO properties as well as the second order hyperpolarizability of the molecules are found to vary with the extent of π-electron delocalization [51]. All these molecules, except CM-1 exhibit strong nonlinear absorption at 532 nm which is primarily rooted in RSA with partial contribution from TPA. A good optical limiting of nanosecond pulses has been observed in these molecules. The compound 2H chromene-2-thione (CM-2) possesses a very high $\chi^{(3)}$ of the order of ~7.4×10^{-12} (esu) which is comparable with the values obtained for ZnTAP by Henari et al. [52] and that of 4-(N, N-diethylamino)-4′-nitrostilbene (DEANS) crystals measured with Third Harmonic Generation technique [53]. A good comparison is obtained through Z-scan and DFWM techniques. Future venture on these compounds includes femtosecond response studies in solution and thin film forms.

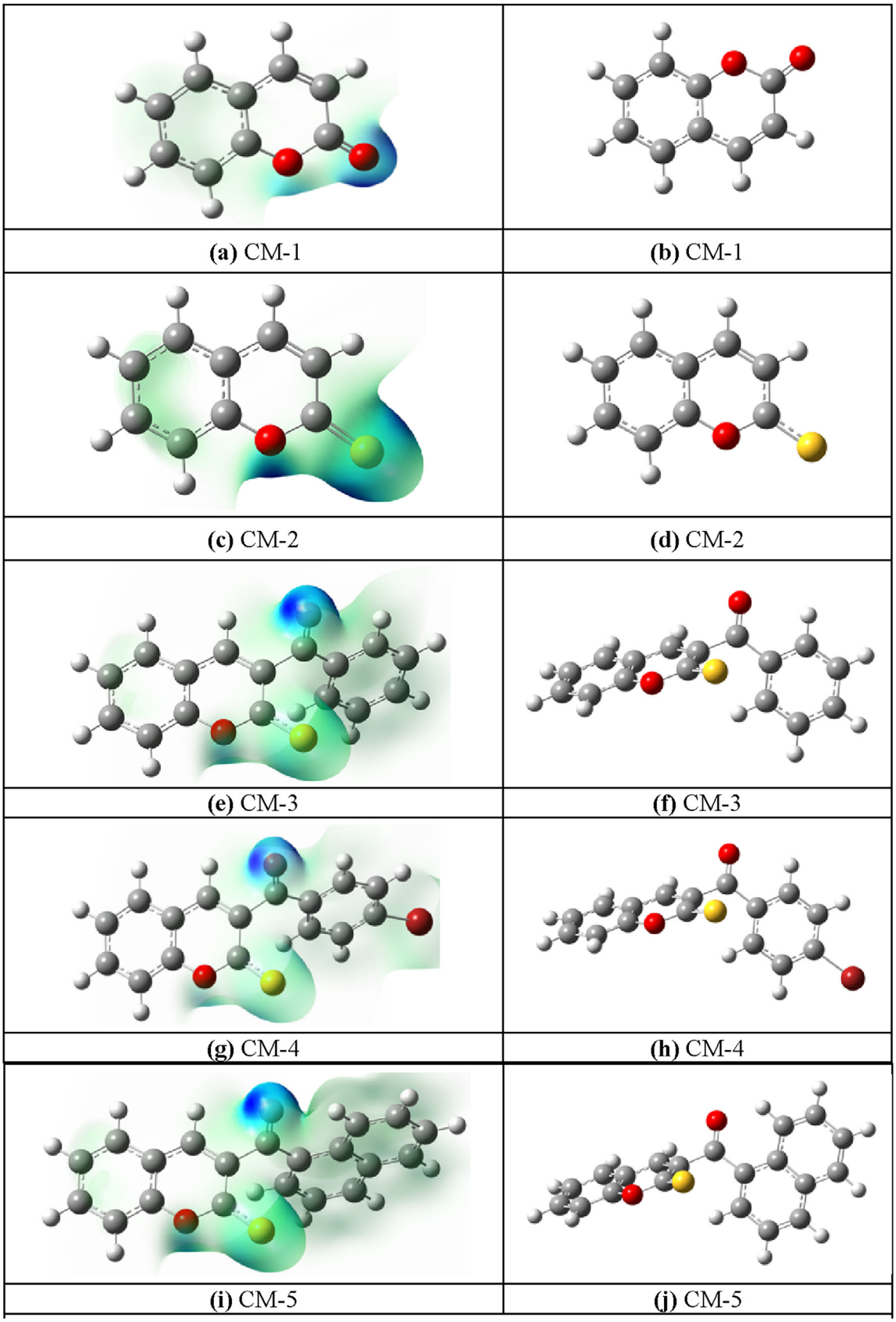

Fig. 10. Molecular Electrostatic Surface Potential mapping of compounds CM-1 to CM-5. Images given at the left hand side show the ESP mapping and the right side pictures show the corresponding optimized molecular geometry configurations.

Acknowledgements

The corresponding author acknowledges Dr. P. Parameswaran and Dijo of Bioinorganic Materials Research Laboratory, Department of Chemistry, NIT Calicut for PL measurements. P. M. thanks KSCSTE, Kerala State, India for financial support (project No. 012/SRSPS/2006/CSTE) and the UGC, India for a generous support of a GCMS facility under the innovative program. J.K. thanks Dr. Jayaram of MES College Ponnani for helpful suggestions. Deep gratitude is expressed to Divyasree, Vijisha, Vasudevan and Shiju of nonlinear optics laboratory, NIT Calicut for fruitful discussions and creative suggestions.

References

[1] L. Dalton, Nonlinear Optical Polymeric Materials: from Chromophore Design to Commercial Applications, Advances in Polymer Science, 158, Springer-Verlag, 2002, pp. 1–86.
[2] L.R. Dalton, W.H. Steier, B.H. Robinson, C. Zhang, A. Ren, S. Garner, A. Chen, T. Londergan, From molecules to opto-chips: organic electro-optic materials, J. Mater. Chem. 9 (1999) 1905–1920.
[3] J.L. Bredas, C. Adant, P. Tackx, A. Persoons, B.M. Pierce, Third-order nonlinear optical response in organic materials: theoretical and experimental aspects, Chem. Rev. 94 (1) (1994) 243–278.
[4] R.R. Tykwinski, U. Gubler, R.E. Martin, F. Diederich, C. Bosshard, P. Gunter, Structure–property relationships in third-order nonlinear optical chromophores, J. Phys. Chem. B 102 (23) (1998) 4451–4465.
[5] Y.H. Pao, P.M. Rentzepis, Multiphoton absorption and optical-harmonic generation in highly absorbing molecular crystals, J. Chem. Phys. 43 (1965) 1281–1291.
[6] P.M. Rentzepis, Y.H. Pao, Laser induced optical second harmonic generation in organic crystals, Appl. Phys. Lett. 5 (1964) 156.
[7] G.I. Stegeman, E.M. Wright, N. Finlayson, R. Zanoni, C.T. Seaton, Third order nonlinear integrated optics, J. Light Wave Technol. 6 (1988) 953–970.
[8] C. Halvorson, T.W. Hagler, D. Moses, Y. Cao, A.J. Heeger, Conjugated polymers with degenerate ground state-the route to high performance third-order nonlinear optical response, Chem. Phys. Lett. 4 (1992) 364–368.
[9] G. de la Torre, P. Vazquez, F. Agullao Lopez, T. Torres, Phthalocyanines and related compounds: organic targets for nonlinear optical applications, J. Mater. Chem. 8 (1998) 1671–1683.
[10] S.G. Roh, N.S. Baek, K.S. Hong, H.K. Kim, Synthesis and photophysical properties of luminescent lanthanide complexes based on coumarin-3-carboxylic acid for advanced photonic applications, Bull. Korean Chem. Soc. 25 (3) (2004) 343–344.
[11] S. Senthilkumar, S. Nath, H. Pal, Photophysical properties of coumarin-30 dye in aprotic and protic solvents of varying polarities, Photochem. Photobiol. 80 (1) (2004) 104–111.
[12] Z.S. Wang, K. Hara, Y. Dan-oh, C. Kasada, A. Shinpo, S. Suga, H. Arakawa, H. Sugihara, Photophysical and photo- electrochemical properties of a coumarin dye, J. Phys. Chem. B 109 (9) (2005) 3907–3914.
[13] D. Egan, R.O. Kennedy, E. Moran, D. Cox, E. Prosser, R.D. Thornes, The pharmacology, metabolism, analysis, and applications of Coumarin and Coumarin-related compounds, Drug Metab. Rev. 22 (5) (1990) 503–529.
[14] M.S. Abdel-Mottaleb, M.S. Antonious, M.M. Abo Ali, L.F.M. Ismail, B.A. El-Sayed, A.M.K. Sherief, Photophysics and dynamics of coumarin laser dyes and their analytical implications, Proc. Indian Acad. Sci. Chem. Sci. 104 (2) (1992) 185–196.
[15] Xin-Mei Peng, Guri L.V. Damu, He Zhou, Cheng, Current developments of Coumarin compounds in medicinal chemistry, Curr. Pharm. Des. 19 (21) (2013) 3884–3930.
[16] S.R. Trenor, A.R. Shultz, B.J. Love, T.E. Long, Coumarins in polymers: from light harvesting to photo-cross-linkable tissue scaffolds, Chem. Rev. 104 (6) (2004) 3059–3078.
[17] D. Gindre, K. Iliopoulos, O. Krupka, M. Evrard, E. Champigny, M. Salle, Coumarin-containing polymers for high density non-linear optical data storage, Molecules 21 (2) (2016) 147.
[18] P. Munshi, T.N. Guru Row, Electron density study of 2H-chromene-2-thione, Acta Crystallogr. Sect. B 58 (2002) 1011–1017.
[19] P. Munshi, T.N. Guru Row, 2H-Thiochromen-2-one, Acta Crystallogr. Sect. E 58 (2002) 353–354.
[20] K.N. Sharafudeen, A. Adithya, S. Vijayakumar, P. Sudheesh, B. Kalluraya, K. Chandrasekharan, Multiphoton absorption process and self-focusing effect in coumarin derivative doped PMMA films by Z-scan and optical limiting studies, Curr. Appl. Phys. 11 (2011) 1089–1093.
[21] R.K. Verma, G.K. Verma, K. Raghuvanshi, M.S. Singh, An expedient route to highly functionalized 2H-chromene-2-thiones via ring annulation of β-oxo-dithioesters catalyzed by $InCl_3$ under solvent-free conditions, Tetrahedron 67 (2011) 584–589.
[22] B.D. Wagner, The use of Coumarins as environmentally-sensitive fluorescent probes of heterogeneous inclusion systems, Molecules 14 (2009) 210–237.
[23] M. Szymański, A. Maciejewski, J. Kozłowski, J. Koput, Photophysics of the S_2 State of Thiocoumarin: a vibrationally unequilibrated luminophore, J. Phys. Chem. A 102 (4) (1998) 677–683.
[24] J.R. Lakowicz, Principles of Fluorescence Spectroscopy, third ed., Springer, Singapore, 2006.
[25] V. Meerwall, A least-squares spectral curve fitting routine for strongly overlapping Lorentzian or Gaussians, Comput. Phys. Commun. 9 (1975) 117–128.
[26] P.B. Chapple, J. Staromlynska, J.A. Hermann, T.J. Mckay, R.G. Mcduff, Single-beam Z-scan: measurement techniques and analysis, J. Nonlinear Opt. Phys. Mater. 06 (1997) 251–293.
[27] E.W. Van Stryland, M. Sheik-Bahae, Characterization Techniques and Tabulations for Organic Nonlinear Materials, Marcel Dekker, Inc, 1998, pp. 655–692.
[28] Y. Gao, X. Zhang, Y. Li, H. Liu, Y. Wang, Q. Chang, W. Jiao, Y. Song, Saturable absorption and reverse saturable absorption in platinum nanoparticles, Opt. Commun. 251 (2005) 429–433.
[29] B. Anand, S.R. Krishnan, R. Podila, S.S. Sankara Sai, A.M. Rao, R. Philip, The role of defects in the nonlinear optical absorption behaviour of carbon and ZnO nanostructures, Phys. Chem. Chem. Phys. 16 (2014) 8168–8177.
[30] M. Sheik-Bahae, A.A. Said, T.H. Wei, D.J. Hagan, E.W. Van Stryland, Sensitive measurement of optical nonlinearities using a single beam, IEEE J. Quantum Electron. 26 (4) (1990) 760–769.
[31] S. Couris, E. Koudoumas, A.A. Ruth, S. Leach, Concentration and wavelength dependence of the effective third-order susceptibility and optical limiting of C_{60} in toluene solution, J. Phys. B Atom., Mol. Opt. Phys. 28 (1995) 4537–4554.
[32] X. Liu, S. Guo, H. Wang, L. Hou, Theoretical study on the closed-aperture Z-scan curves in the materials with nonlinear refraction and strong nonlinear absorption, Opt. Commun. 197 (2001) 431–437.
[33] R.L. Sutherland, Handbook of Nonlinear Optics, second ed., Marcel Dekker, NewYork, 2003.
[34] R.Gower Caro, C. Malcolm, Phase conjugation by degenerate four-wave mixing in absorbing media, IEEE J. Quantum Electron. 18 (1982) 1376–1380.
[35] T. Sakaguchi, Y. Shimizu, T. Fukumi, A. Nagata, Third order nonlinear optical susceptibilities of solutions of some mesogenic metallotetraphenylporphyrins by nanosecond degenerate four-wave mixing method, Chem. Lett. 15 (1992) 281–284.
[36] J.S. Shirk, G.S. Richard, F.J. Pong, W. Snow, Optical limiter using a lead phthalocyanines, Appl. Phys. Lett. 63 (1993) 1880–1882.
[37] X. Sun, R.Q. Yu, G.Q. Xu, T.S.A. Hor, W. Ji, Broadband optical limiting with multi-walled carbon nanotubes, Appl. Phys. Lett. 73 (1998) 3632–3634.
[38] L.W. Tutt, T.F. Boggess, A review of optical limiting mechanism and devices using organics, fullerenes, semiconductors, and other materials, Prog. Quantum Electron. 17 (1993) 299–338.
[39] W.M. Moore, M. Ketchum, The quenching effect of naphthalene on the photoreduction of benzophenone, J. Am. Chem. Soc. 84 (8) (1962) 1368–1371.
[40] E. Abuin, E.A. Lissi, Kinetics of the type I photocleavage of aliphatic ketones, J. Photochem. 6 (1977) 1–8.
[41] N. Matsuzawa, D.A. Dixon, Semiempirical calculations of the polarizability and second-order hyperpolarizability of fullerenes (C60 and C70) and model aromatic compounds, J. Phys. Chem. 96 (15) (1992) 6241–6247.
[42] A.G. Astill, Material figures of merit for non-linear optics, Thin Solid Films 204 (1) (1991) 1–17.
[43] D.L. Torre, P. Vazquez, L.F. Agullo, T. Torres, Phthalocyanines and related compounds: organic targets for nonlinear optical applications, J. Mater. Chem. 8 (8) (1998) 1671–1683.
[44] K. Ogawa, T. Zhang, K. Yoshihara, Y. Kobuke, Large third-order optical nonlinearity of self-assembled porphyrin oligomers, J. Am. Chem. Soc. 124 (2002) 22–23.
[45] W. Blau, H. Byrne, W.M. Dennis, J.M. Kelly, Reverse saturable absorption in tetraphenylporphyrins, Opt. Commun. 56 (1985) 25–29.
[46] S.S. Harilal, C.V. Bindhu, V.P.N. Nampoori, C.P.G. Vallabhan, Optical limiting and thermal lensing studies in C60, J. Appl. Phys. 86 (3) (1999) 1388–1392.
[47] M. J. Frisch, G. W. Trucks, H. B. Schlegel, G. E. Scuseria, M. A. Robb, J. R. Cheeseman, G. Scalmani, V. Barone, B. Mennucci, G. A. Petersson, H. Nakatsuji, M. Caricato, X. Li, H. P. Hratchian, A. F. Izmaylov, J. Bloino, G. Zheng, J. L. Sonnenberg, M. Hada, M. Ehara, K. Toyota, R. Fukuda, J. Hasegawa, M. Ishida, T. Nakajima, Y. Honda, O. Kitao, H. Nakai, T. Vreven, J. J. A. Montgomery, J. E. Peralta, M. B. F. Ogliaro, J. J. Heyd, E. Brothers, K. N. Kudin, V. N. Staroverov, R. Kobayashi, J. Normand, K. Raghavachari, A. Rendell, J.C. Burant, S. S. Iyengar, J. Tomasi, M. Cossi, N. Rega, J. M. Millam, M. Klene, J. E. Knox, J. B. Cross, V. Bakken, C. Adamo, J. Jaramillo, R. Gomperts, R. E. Stratmann, O. Yazyev, A. J. Austin, R. Cammi, C. Pomelli, J.W. Ochterski, R. L. Martin, K. Morokuma, V. G. Zakrzewski, G. A. Voth, P. Salvador, J. J. Dannenberg, S. Dapprich, A. D. Daniels, Ö. Farkas, J. B. Foresman, J.V. Ortiz, J. Cioslowski, D. J. Fox, Gaussian, Inc., Wallingford CT, (2009).
[48] A.D. Becke, Density-functional thermochemistry. III, the role of exact exchange, J. Chem. Phys. 98 (7) (1993), 5648–565.
[49] C. Lee, W. Yang, R.G. Parr, Development of the Colle-Salvetti correlation-energy formula into a functional of the electron density, Phys. Rev. B 37 (2) (1998) 785–789.
[50] M. Agostinha, R. Matos, Clara C.S. Sousa, Victor M.F. Morais, Experimental and computational thermochemistry of the isomers: chromanone, 3-

isochromanone, and dihydrocoumarin, J. Chem. Thermodyn. 41 (3) (2009) 308–314.
[51] S.R. Marder, J.E. Sohn, G.D. Stucky, Materials for Nonlinear Optics Chemical Perspectives, American Chemical Society, Washington DC, 1991.
[52] F.Z. Henari, W.J. Blau, L.R. Milgrom, G. Yahioglu, D. Phillips, J.A. Lacey, Third-order optical non-linearity in Zn(II) complexes of 5,10,15,20-tetraarylethynyl-substituted porphyrins, Chem. Phys. Lett. 267 (1997) 229–233.
[53] T. Kurihara, H. Kobayashi, K. Kubodera, T. Kaino, $\chi^{(3)}$ evaluation for the molecular crystals of 4-(N,N-diethylamino)-4′-nitrostilbene (DEANS), Chem. Phys. Lett. 165 (1990) 171–174.